Bulletin of Electrical Engineering and Informatics
Vol. 15, No. 4, August 2026, pp. 3646~3659
ISSN: 2302-9285, DOI: 10.11591/eei.v15i4.11246

Fractional Perona–Malik-based processing for noise reduction and structure preservation in red, green, blue Pap smear images

Syaiful Anam[1], Normi Abdul Hadi[2], Avin Maulana[1], Indah Yanti[1], Suhaila Abd Halime[2]
[1]Department of Mathematics, Faculty of Science, Technology, and Mathematics, Brawijaya University, Malang, Indonesia
[2]Center of Mathematical Sciences, Faculty of Computer and Mathematical Sciences, Universiti Teknologi MARA, Selangor, Malaysia

Article Info

Article history:

Received Aug 20, 2025
Revised May 2, 2026
Accepted Jul 9, 2026

Keywords:

Anisotropic diffusion filtering
Cervical cancer
Fractional Perona–Malik diffusion
Noise reduction
Pap smear image

ABSTRACT

Cervical cancer screening relies heavily on Pap smear analysis, yet image noise, low contrast, and overlapping cellular structures continue to limit diagnostic accuracy and the performance of automated systems. This study introduces a fractional Perona–Malik diffusion (FPMD) framework that extends the classical anisotropic diffusion model using fractional-order operators to achieve more flexible, edge-sensitive smoothing. The method is applied to red, green, blue (RGB) Pap smear images and benchmarked against classical Perona–Malik diffusion (PMD) and conventional filters using entropy, blind/referenceless image spatial quality evaluator (BRISQUE), and edge preservation index (EPI). FPMD yields substantial improvements, achieving the lowest BRISQUE score (18.88) and the highest EPI values (>0.92) across all channels, indicating superior structural preservation and perceptual quality. While classical PMD produces slightly higher entropy, it introduces artifacts that degrade visual realism. FPMD provides a more controlled enhancement, producing diagnostically meaningful contrast and clearer cytological boundaries. These results highlight its potential as a robust preprocessing tool for both manual assessment and artificial intelligence (AI)-assisted cervical cancer screening.

Corresponding Author:

Syaiful Anam
Department of Mathematics, Faculty of Science, Technology, and Mathematics, Brawijaya University
Veteran Street, Malang, Indonesia
Email: syaiful@ub.ac.id

1. INTRODUCTION

Cervical cancer is the second most common malignancy among women in Indonesia, with an estimated 36,633 new cases and 21,033 deaths annually [1], [2]. Alarmingly, around 80% are diagnosed at advanced stages (III–IV), predominantly in women over 45 years [3]. Low screening rates, limited awareness, and lack of human papillomavirus (HPV) vaccination access exacerbate late detection [4], [5]. The World Health Organization (WHO) therefore advocates enhanced screening strategies and awareness campaigns to reduce the cervical cancer burden.

Early detection significantly improves survival, with five-year survival rates reaching 80–90% when diagnosed promptly [6], [7]. Conventional tests such as Pap smear and HPV testing remain vital in identifying precancerous lesions [8]. Regular Pap smear screening alone can reduce incidence and mortality by 60–90% [9] and, compared with HPV deoxyribonucleic acid (DNA) testing, offers direct cellular observation that is cost-effective in resource-limited settings [9]-[11]. Combining both tests further improves accuracy and risk stratification [12], [13].

However, Pap smear image analysis faces obstacles including noise, low contrast, and overlapping cells, which compromise interpretation [14], [15]. Enhancement techniques such as histogram equalization and

contrast stretching improve visualization but often fail to preserve cytological detail [16]. Existing enhancement methods may increase apparent clarity but commonly introduce artifacts or over-enhance certain regions, leading to loss of diagnostic structures such as nuclear boundaries and cytoplasmic textures. More advanced filters, including bilateral filtering and anisotropic diffusion, provide edge-preserving smoothing, yet they may still struggle to maintain subtle cytological features required for accurate screening [14].

Recent studies have further demonstrated that image preprocessing strongly influences the performance of artificial intelligence (AI)-assisted cervical cancer analysis. Hybrid preprocessing approaches combining classical Perona–Malik diffusion (PMD) and contrast limited adaptive histogram equalization (CLAHE) have been shown to significantly enhance Pap smear image quality [17]. In parallel, filter-based enhancement methods such as Gaussian, bilateral, and median filtering have been evaluated in convolutional neural network (CNN)-based decision support systems, where Gaussian blur achieved the best diagnostic performance, underscoring the importance of preprocessing choices [18]. Median filtering has also been integrated with U-Net architectures for nucleus and cytoplasm segmentation, yielding segmentation accuracies above 90%, although such approaches rely on fixed, integer-order filters and limited adaptivity [19].

Among diffusion-based approaches, the PMD filter is widely recognized as a cornerstone edge-preserving technique in medical image enhancement. By modulating diffusion according to image gradients, PMD selectively smooths homogeneous regions while inhibiting diffusion across edges, enabling superior preservation of nuclei and cytoplasmic boundaries compared with conventional linear filters [20], [21]. However, classical PMD relies on an integer-order formulation, which limits its ability to preserve fine-scale cytological details and may cause blurring in regions with subtle morphological variations. This limitation motivates the development of enhanced diffusion models capable of more adaptive and structure-sensitive smoothing.

Building on this, integrating fractional-order derivatives into PMD introduces greater adaptability in image smoothing and edge preservation [22], [23]. Fractional-order diffusion improves edge definition, reduces background noise, and enhances texture representation, enabling more accurate detection of abnormal cells [24], [25]. Its benefits extend to AI-based classification models, as higher-quality inputs improve learning efficiency [26], [27].

Despite the growing body of research on image enhancement for Pap smear analysis, several limitations remain. Existing preprocessing approaches predominantly rely on integer-order diffusion or fixed-parameter filtering techniques, which may lack sufficient adaptability to preserve fine cytological structures while effectively suppressing noise. Furthermore, the application of fractional-order anisotropic diffusion specifically for red, green, blue (RGB) Pap smear images has not been systematically investigated, particularly in terms of perceptual quality (BRISQUE), edge preservation index (EPI), and information richness (entropy). The influence of the fractional-order parameter on diagnostic image quality also remains underexplored. Therefore, there is a clear need for a more flexible diffusion-based framework that can balance noise reduction and structural preservation in cervical cytology images.

For these reasons, this study proposes a preprocessing method based on fractional Perona–Malik diffusion (FPMD) for enhancing RGB Pap smear images. By incorporating fractional-order calculus into the traditional PMD framework, FPMD achieves adaptive, edge-preserving smoothing that improves nuclei and cytoplasmic boundary visibility. The main contributions are: i) formulation of a fractional anisotropic diffusion model for cervical cytology, ii) quantitative evaluation using entropy, BRISQUE, and EPI, and iii) demonstration of improved diagnostic quality to support effective screening in resource-limited healthcare settings.

2. METHOD

There are 4 stages of method involved in this study as in Figure 1. The stages start with image data collection, then the process proceed to data preprocessing before the FPMD filter for enhancing Pap smear image. Lastly, the process of evaluation and interpretation of enhanced image was implemented. In the process of the data preprocessing stage, there has two steps involved which are the implementation of CLAHE and image normalization. The purpose of image normalization is to improve the efficiency of computation process.

2.1. Data collection

This study employs the Pap Smear Single Cell Image Dataset from Kaggle, which contains 917 RGB images of cervical cells prepared for classification and pattern recognition in cancer screening. The dataset includes five cell types, dyskeratotic, koilocytotic, metaplastic, parabasal, and superficial-intermediate, each representing different abnormality levels, making it highly relevant for early detection research.

For this study, five images from each cytological class were randomly selected, with representative examples shown in Figure 2. Figure 2(a) presents a dyskeratotic cell with dense orangeophilic cytoplasm and a small hyperchromatic nucleus. Figure 2(b) shows a koilocytotic cell characterized by a distinct perinuclear

halo and an enlarged, irregular nucleus. Figure 2(c) depicts a metaplastic cell with a round-to-polygonal shape, dense cyanophilic cytoplasm, and a relatively uniform central nucleus. Figure 2(d) shows a small parabasal cell with scant cytoplasm and a high nucleus-to-cytoplasm ratio, whereas Figure 2(e) presents larger superficial–intermediate cells with abundant cytoplasm and relatively small nuclei. These variations in cell size, shape, colour, nuclear structure, and nucleus-to-cytoplasm ratio illustrate the complexity of cervical cytology. Therefore, FPMD is important for reducing image noise while preserving diagnostically relevant features, such as nuclear contours, perinuclear halos, cytoplasmic boundaries, and fine cellular textures.

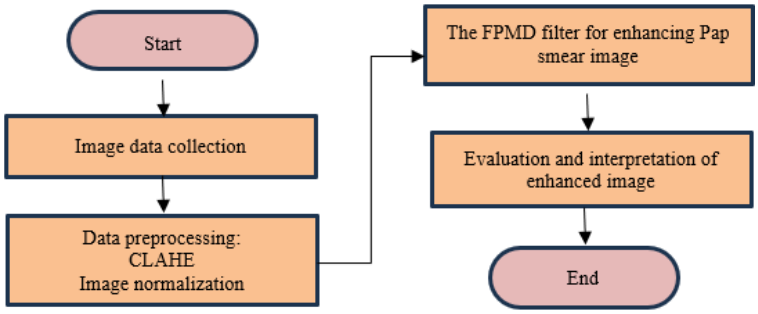

Figure 1. Stages of method

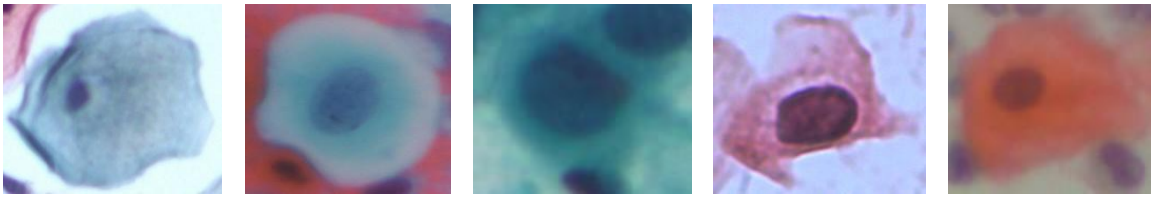

(a) (b) (c) (d) (e)

Figure 2. Example of dataset; (a) dyskeratotic, (b) koilocytotic, (c) metaplastic, (d) parabasal, and (e) superficial-intermediate

2.2. Data preprocessing

Preprocessing is a crucial stage in image analysis to ensure that input data are standardized, noise-reduced, and suitable for subsequent enhancement. In this study, Pap smear images were imported in RGB mode to preserve cytological information across the RGB channels, which were processed independently since each contains unique diagnostic features and is affected by noise differently [26]. For contrast enhancement, the CLAHE method was applied [28], and its continued relevance in modern medical image enhancement has been reported in recent studies [29]. CLAHE improves local contrast by dividing images into tiles, applying histogram equalization to each tile, and merging them through bilinear interpolation, while a clip limit prevents over-amplification of noise [28]. This approach is particularly effective in medical imaging where low contrast and uneven illumination are common. After CLAHE, each channel was normalized to a floating-point range [0,1] by mapping pixel intensities from their original 8-bit scale (0–255) [30]. Normalization improves numerical stability and ensures consistent input for diffusion-based enhancement. Finally, the preprocessed channels were passed to the enhancement stage (classical PMD or fractional PMD) and recombined to produce the final enhanced RGB image.

2.3. Fractional Perona–Malik diffusion

The PMD filter, introduced in 1990, is a nonlinear anisotropic method for denoising while preserving edges [31]. In recent years, the original Perona–Malik framework has been extended toward adaptive and learnable diffusion formulations, including models with trainable diffusion coefficients for improved medical image denoising performance [25]. These developments highlight the ongoing evolution of anisotropic diffusion methods and motivate further extensions, such as the proposed fractional-order formulation. Unlike isotropic filters such as Gaussian blur, which smooth uniformly, PMD selectively smooths homogeneous regions and inhibits diffusion across edges, making it valuable in medical imaging. The classical PMD is defined as (1):

$$\frac{\partial u}{\partial t} = \nabla \cdot (c(x,y,t)\nabla u) \quad (1)$$

where $u(x,y,t)$ is image intensity, ∇u is the gradient, $\nabla \cdot$is the divergence, and $c(x,y,t)$ the diffusion coefficient. To reduce blurring, $c(\cdot)$ is defined as (2):

$$c(\nabla u) = exp(-k \mid \nabla u \mid^2) \quad (2)$$

with k controlling edge sensitivity. The discrete form of (1) could be defined by (3):

$$u_{i,j}(t+1) = u_{i,j}^t + dt \cdot (c_N \Delta N + c_S \Delta S + c_E \Delta E + c_W \Delta W) \quad (3)$$

where $\Delta N, \Delta S, \Delta E, \Delta W$ are directional gradients and c_N, c_S, c_E, c_W the diffusion coefficients. PMD effectively smooths noise and artifacts but, due to its integer-order formulation, may blur fine details if parameters are not optimally chosen.

To overcome this, the FPMD introduces fractional calculus. The Grünwald–Letnikov (GL) scheme is used to approximate fractional derivatives, capturing non-local structural continuity and subtle textures [32]. The FPMD model is formulated as (4):

$$\frac{\partial^\alpha u(x,y,t)}{\partial t^\alpha} = \nabla^\alpha \cdot (c(x,y,t)\nabla^\alpha u(x,y,t)), \quad \alpha \in (0,1] \quad (4)$$

with diffusion coefficient defined by (5):

$$c(\mid \nabla^\alpha u \mid) = exp\left(-\left(\frac{|\nabla^\alpha u|}{k}\right)^2\right) \quad (5)$$

Here, α controls the fractional order, dt the time step, and k edge sensitivity. In implementation, GL finite differences approximate fractional operators. Each RGB channel is processed independently with parameters $\alpha = 0.8$, $dt = 0.2$, $k = 0.05$, and 25 iterations, before recombining into the enhanced RGB image. The selected parameters ($\alpha = 0.8$, $\Delta t = 0.2$, $k = 0.05$, and 25 iterations) were determined based on stability considerations and preliminary experiments, which showed a favorable trade-off between noise suppression and edge preservation across different cytological classes.

Based on the workflow illustrated in Figure 1 and the mathematical formulation described above, Algorithm 1 summarizes the complete implementation of the proposed FPMD method for RGB Pap smear images. The algorithm details the preprocessing steps, the per-channel fractional diffusion process using the GL scheme, and the subsequent evaluation using entropy, EPI, and BRISQUE metrics.

Algorithm 1. FPMD for RGB Pap smear images

Input:

RGB image I(uint8); parameters: fractional order α, time step Δt, edge sensitivity k, number of iterations N, GL weight length L; CLAHE parameters (clipLimit, tileGridSize)

Output:

Enhanced RGB image $\hat{I}$; evaluation metrics: Entropy, EPI, BRISQUE

1. Read RGB image I
2. Split channels: $IR, IG, IB \leftarrow split(I)$
3. for each channel $C \in \{IR, IG, IB\}$ do
   a. $C \leftarrow CLAHE(C)$
   b. $C \leftarrow normalize(C)$ // intensity mapped to [0, 1]
   c. GL weights: $w_0 \leftarrow 1$
   d. for $m = 1$ to L do
      i. $w_m \leftarrow w_{m-1} \cdot \left((\alpha - (m-1))/m\right) \cdot (-1)$
   e. end for
   f. $U \leftarrow C$ // initialization
   g. for t = 1 to N do
      i. Compute fractional gradients using GL scheme: $D_x^\alpha(U), D_y^\alpha(U)$
      ii. Compute gradient magnitude: $G \leftarrow sqrt\left(\left(D_x^\alpha(U)\right)^2 + \left(D_y^\alpha(U)\right)^2\right)$
      iii. Compute diffusion coefficient (Perona–Malik): c ← exp(−(G / k)²)
      iv. Update image:
      v. $U \leftarrow U + \Delta t \cdot div\left(c \cdot \left[D_x^\alpha(U), D_y^\alpha(U)\right]\right)$
   h. end for
   i. C_enh ← U
4. end for
5. Merge channels: $\hat{I} \leftarrow merge\,(IR\_enh, IG\_enh, IB\_enh)$

6. Compute evaluation metrics: $Entropy\,(\hat{I}R,\hat{I}G,\hat{I}B)$, $EPI \leftarrow SSIM(SobelEdges(I), SobelEdges(\hat{I}))$, $BRISQUE(\hat{I})$
7. Return $\hat{I}$ and metrics

All experiments were conducted using Google Colaboratory, implemented in Python (version 3.x). The computational environment utilized the default Colab configuration, running on a cloud-based workstation with an Intel Xeon CPU and approximately 12–16 GB of RAM, which ensures reproducibility and accessibility of the proposed method.

2.4. Evaluation metrics and interpretation

Since the material is related, the metrics of entropy, EPI, BRISQUE, and visual evaluation were used to assess the effectiveness of the suggested FPMD technique.

2.4.1. Entropy

Entropy quantifies the information content or textural variability of an image. Higher entropy reflects greater detail and structural preservation after enhancement [29].

2.4.2. Edge preservation index

EPI is a key quantitative metric for evaluating image processing performance, particularly in preserving edge sharpness and structural integrity during denoising, fusion, and enhancement [33]. Higher EPI values indicate better edge retention, which is critical for maintaining diagnostic features.

2.4.3. Blind/referenceless image spatial quality evaluator score

BRISQUE is a reference-free perceptual quality metric that measures both distortion and naturalness without requiring a ground truth image [30]. While BRISQUE remains widely adopted in medical image enhancement studies, recent advances in blind image quality assessment increasingly leverage deep learning architectures for perceptual modelling [34], highlighting the evolution of NR-IQA frameworks beyond traditional statistical feature-based approaches. Lower BRISQUE scores indicate better human-perceived visual quality [30].

2.4.4. Visual assessment

A qualitative comparison of original, PMD-enhanced, and FPMD-enhanced images shows that FPMD provides clearer nuclear boundaries, sharper cytoplasmic textures, and stronger background contrast, resulting in superior visual sharpness and diagnostic interpretability.

For evaluation and interpretation, the proposed FPMD method is compared with three representative preprocessing approaches from recent studies. These include hybrid PMD–CLAHE for Pap smear enhancement [17], median filtering [19], and conventional filter-based preprocessing using Gaussian, bilateral, and median filters [18]. The comparison demonstrates that FPMD provides more adaptive and structure-preserving enhancement than existing integer-order and fixed-parameter filtering methods.

3. RESULTS AND DISCUSSION

This section presents the outcomes of the proposed FPMD approach in comparison with conventional filters and the classical PMD. Performance was evaluated both quantitatively, using established image quality metrics, and qualitatively through visual inspection, focusing on three key aspects in Pap smear image analysis: noise suppression, edge preservation, and perceptual quality [34]. Three objective metrics were employed: BRISQUE, entropy, and EPI. BRISQUE quantifies perceptual naturalness, with lower scores indicating better quality; EPI, derived from SSIM between Sobel edge maps, measures edge preservation; and entropy reflects information richness, with higher values indicating improved texture and contrast.

Consistent with these comparisons, the quantitative results demonstrate that the proposed FPMD method outperforms hybrid PMD–CLAHE–based enhancement [17], median filtering–based approaches [19], and conventional filter-based preprocessing methods [18] in terms of perceptual quality and edge preservation. While these existing approaches improve contrast and reduce noise, their reliance on integer-order or fixed-parameter formulations limits adaptivity, whereas FPMD achieves lower BRISQUE scores and higher EPI values, demonstrating more effective preservation of diagnostically relevant cytological structures. To further substantiate these comparative findings, the following analysis examines the influence of the fractional-order parameter on BRISQUE, EPI, and entropy values across different cytological classes.

Figure 3 evaluates the sensitivity of the proposed FPMD method to different fractional-order values across the five cytological classes using three complementary image-quality metrics: perceptual quality, edge

preservation, and information richness. Analysis of the fractional parameter α in FPMD shows that increasing α from 0.1 to 0.5 consistently raises BRISQUE scores Figure 3(a), implying reduced perceptual quality due to over smoothing. The lowest BRISQUE scores, and hence best visual quality, are achieved at $\alpha = 0.1$. Similarly, EPI values decline with increasing α Figure 3(b), confirming progressive edge loss, most notably for the metaplastic class, while other classes retain higher edge integrity. Entropy Figure 3(c) remains stable across most classes, though the metaplastic class shows a sharp decline for $\alpha > 0.6$, indicating information loss. Overall, the interval $\alpha = 0.1 - 0.3$ provides the best compromise, enhancing contrast and reducing noise while maintaining edges and texture. Another important limitation is the use of manually selected diffusion and fractional-order parameters. This motivates the development of automated parameter-tuning mechanisms, for example Bayesian optimization or evolutionary search, to ensure consistent performance across varying cytological characteristics.

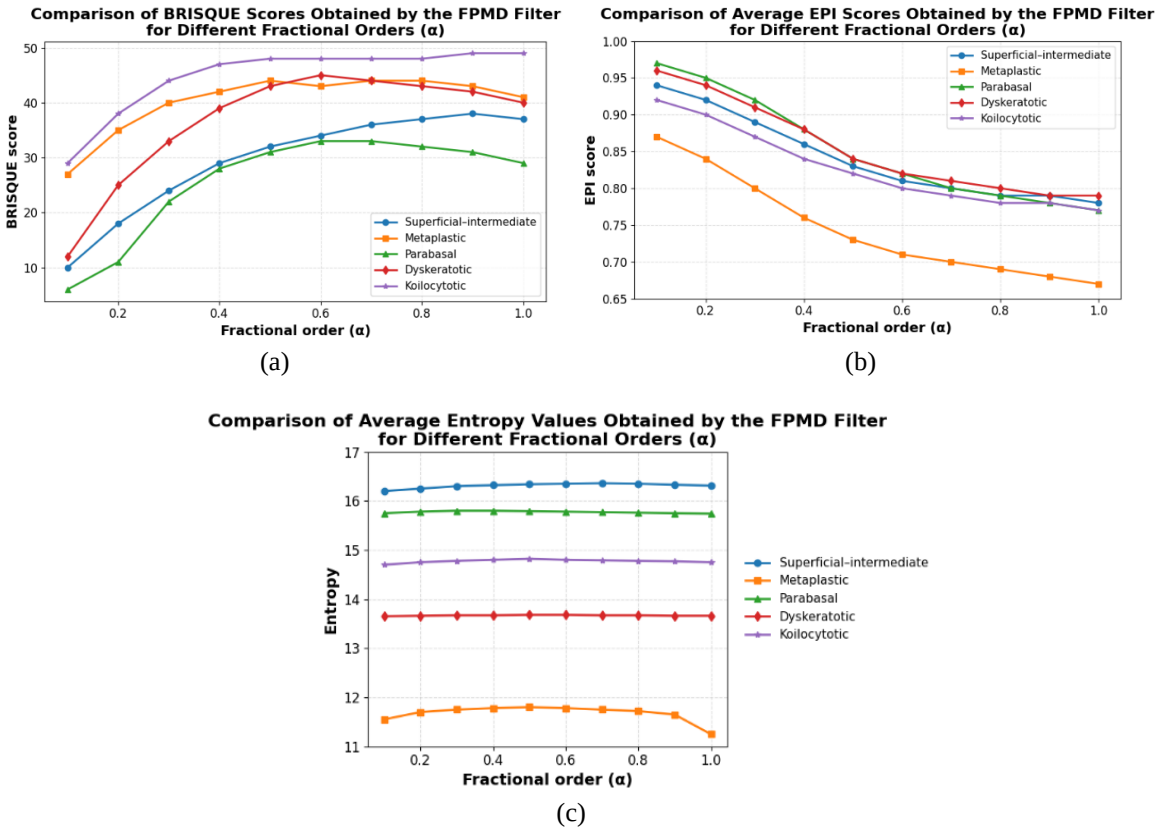

Figure 3. FPMD performance at different fractional-order values; (a) BRISQUE, (b) EPI, and (c) entropy

The improved performance of the proposed FPMD model compared with the classical integer-order PMD can be explained by several theoretical properties of the fractional diffusion formulation, including the nonlocal gradient operator, the nonlinear diffusion coefficient, the stability of the numerical scheme, and the spectral characteristics of fractional differentiation. In the classical PMD model, diffusion is governed by (1). Because the diffusion process relies on the local gradient ∇u, the gradient magnitude is computed only from immediate neighboring pixels. This locality makes the gradient estimation highly sensitive to noise, since random fluctuations in pixel intensity may produce artificial gradients that disturb the diffusion process. To address this limitation, the proposed model replaces the local gradient with a fractional-order gradient operator. In practice, the fractional gradient can be approximated using the GL formulation in (6):

$$\nabla^{\alpha} u(x) \approx \sum_{k=0}^{M} (-1)^k \binom{\alpha}{k} u(x - kh), 0 < \alpha < 1 \quad (6)$$

Unlike the classical derivative, this formulation introduces nonlocal spatial interactions, since the derivative at position x depends on a weighted combination of intensities from a broader spatial neighbourhood. The binomial coefficients determine how strongly distant pixels contribute to the derivative. As a result, gradient estimation becomes more robust to random noise because the influence of stochastic fluctuations tends to be averaged across multiple spatial locations. Within this framework, the diffusion

equation becomes (4) and the diffusion coefficient is represented by (5). The function $c(|\nabla^{\alpha}u|)$ acts as an edge-stopping mechanism that controls the diffusion strength according to the local fractional gradient magnitude. When the gradient magnitude is small, corresponding to homogeneous regions, the coefficient approaches unity $c(0) = 1$, which allows strong smoothing and effective noise suppression. Conversely, when the gradient magnitude becomes large, the exponential form of the diffusion coefficient rapidly decreases the diffusivity, thereby suppressing diffusion near structural boundaries. This mechanism prevents excessive smoothing and preserves important image edges. The fractional order parameter α further determines the spatial scale of the diffusion process. As $\alpha \to 1$, the fractional derivative converges to the classical gradient,

$$\nabla^{\alpha}u \to \nabla u \tag{7}$$

and the model reduces to the standard PMD formulation. For smaller values of α, however, the derivative incorporates information from a wider spatial neighborhood, which enhances structural continuity while reducing the influence of noise.

From a numerical standpoint, the stability of the discrete diffusion scheme is also an important property. Using an explicit discretization, the iterative update can be written as (8):

$$u_{i,j}^{n+1} = u_{i,j}^{n} + \Delta t\, \nabla \cdot \left(c(|\nabla^{\alpha}u_{i,j}^{n}|)\nabla^{\alpha}u_{i,j}^{n}\right) \tag{8}$$

Because the exponential diffusion coefficient satisfies (9):

$$0 < c(|\nabla^{\alpha}u|) \leq 1 \tag{9}$$

the diffusion flux remains bounded throughout the iterative process. Under the standard Courant–Friedrichs–Lewy stability condition for diffusion equations, the time step must satisfy (10):

$$\Delta t \leq \frac{1}{2d} \tag{11}$$

where d denotes the spatial dimension. This bounded diffusivity ensures that the numerical scheme remains stable during iteration. Compared with the classical integer-order PMD model, the presence of the fractional gradient $\nabla^{\alpha}u$ introduces nonlocal spatial interactions into the diffusion flux. Instead of relying only on immediate neigh boring pixels, the fractional operator incorporates weighted intensity differences from a wider spatial neighbourhood through the GL formulation. This nonlocal interaction effectively smooths stochastic fluctuations in the gradient estimation while preventing abrupt variations in the diffusion flux. As a consequence, the numerical evolution becomes more stable with respect to noise-induced gradients, which are common in Pap smear images. In classical PMD, local noise may produce large gradient magnitudes that lead to unstable or excessive diffusion near edges. In contrast, the fractional operator distributes the gradient information over a larger spatial support, resulting in a more stable diffusion flow that suppresses noise while preserving structural boundaries. Therefore, the combination of bounded exponential diffusivity and the nonlocal fractional gradient produce a numerically stable diffusion scheme that is less sensitive to noise and more effective in maintaining structural continuity than the classical integer-order PMD formulation.

From an energy perspective, the diffusion process can be interpreted as minimizing an energy functional:

$$E(u) = \int_{\Omega} \phi(|\nabla^{\alpha}u|)\, dx \tag{12}$$

where $\phi(\cdot)$ is a potential function related to the diffusion coefficient. For the exponential diffusivity used in this work, the potential function is given by (13).

$$\phi(s) = \frac{k^2}{2}\left(1 - exp\left(-\left(\frac{|\nabla^{\alpha}u|}{k}\right)^2\right)\right) \tag{13}$$

The diffusion equation can therefore be interpreted as the gradient descent flow of this energy functional, meaning that the iterative process progressively reduces the total energy of the image while preserving discontinuities corresponding to meaningful structures. The key difference from the classical Perona–Malik model lies in the definition of the gradient term. In the standard PMD formulation, the energy functional is defined using the local gradient:

$$E_{PMD}(u) = \int_{\Omega} \phi(|\nabla u|)\, dx \tag{14}$$

where the energy depends only on local pixel variations. Consequently, the diffusion process is strongly influenced by local noise fluctuations, which may distort gradient estimation and lead to excessive smoothing near fine structural details.

In contrast, the proposed FPMD model replaces the local gradient with the fractional-order gradient $\nabla^{\alpha}u$. Because the fractional derivative incorporates weighted contributions from a wider spatial neighborhood, the corresponding energy functional becomes inherently nonlocal. This nonlocal formulation stabilizes gradient estimation and reduces the influence of random noise, while maintaining sensitivity to meaningful structural discontinuities. As a result, the energy minimization process suppresses stochastic fluctuations in homogeneous regions while preserving edges and fine cytological structures more effectively than the integer-order PMD model. This theoretical property explains the experimental observations, where the proposed FPMD achieves higher EPI values and lower BRISQUE scores compared with classical PMD, indicating improved structural preservation and perceptual image quality.

Additional insight can be obtained from a spectral analysis of the fractional derivative. In the Fourier domain, the fractional gradient satisfies (15):

$$\mathcal{F}[\nabla^{\alpha}u](\omega) = (i\omega)^{\alpha}\mathcal{F}[u](\omega) \tag{15}$$

This relation indicates that fractional differentiation behaves as a power-law operator in the frequency domain. Compared with integer-order diffusion, which strongly attenuates high-frequency components, fractional diffusion produces a more gradual attenuation across the frequency spectrum. As a result, high-frequency noise is suppressed while intermediate frequency components corresponding to structural edges are preserved.

Taken together, these theoretical properties explain why the proposed FPMD model provides a more balanced trade-off between noise suppression and edge preservation than classical anisotropic diffusion. The nonlocal gradient improves gradient estimation, the nonlinear diffusion coefficient selectively controls smoothing, the numerical scheme remains stable during iteration, and the spectral behavior preserves structural image features. This theoretical behavior explains the observed experimental trends, where the nonlocal fractional operator stabilizes gradient estimation and prevents excessive diffusion near structural boundaries, resulting in higher EPI values and lower BRISQUE scores compared with classical PMD.

Figure 4 compares BRISQUE scores across methods. The original image scores 35.59, classical PMD increases distortion to 55.78, while FPMD achieves 18.88, significantly improving perceptual quality. Among conventional filters, Median (35.18) performs closest to the original, whereas Mean (44.90), Gaussian (42.99), and especially Bilateral (66.85) degrade quality. Thus, FPMD consistently outperforms all methods in perceptual evaluation.

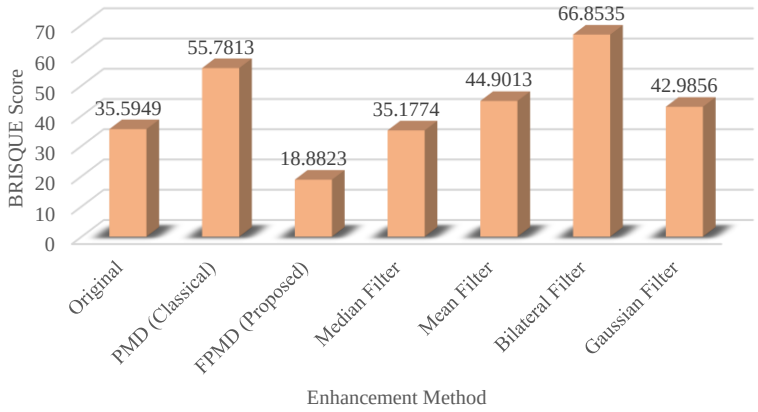

Figure 4. Comparison of the average of BRISQUE Score between FPMD filter method, classical PMD filter method and benchmark filtering methods

Figure 5 compares the average EPI scores of the proposed FPMD filter, the classical PMD filter, and benchmark methods across the Figures 5(a) red, 5(b) green, and 5(c) blue channels. The proposed FPMD consistently achieves the highest values, confirming its superior ability to suppress noise while preserving fine edges. This indicates that FPMD enhances cytological details more effectively across all colour channels, which is essential for accurate segmentation and reliable detection of abnormal cells in Pap smear images.

Table 1 shows that classical PMD achieves the highest entropy values (15.2941 R, 15.0105 G, 14.8250 B), followed closely by the proposed FPMD (15.1451 R, 14.8505 G, 14.6377 B). Conventional filters such as Median, Mean, Bilateral, and Gaussian produce only moderate entropy improvements, while the original images exhibit intrinsically low entropy (6.61 R, 6.46 G, 6.32 B). Although classical PMD produces slightly higher entropy than FPMD, the gain largely reflects excessive contrast amplification, which may introduce artificial details rather than clinically meaningful structures. This effect explains why its perceptual quality (BRISQUE) degrades despite high entropy. In contrast, FPMD provides a more controlled enhancement, achieving a better balance between information richness and perceptual naturalness.

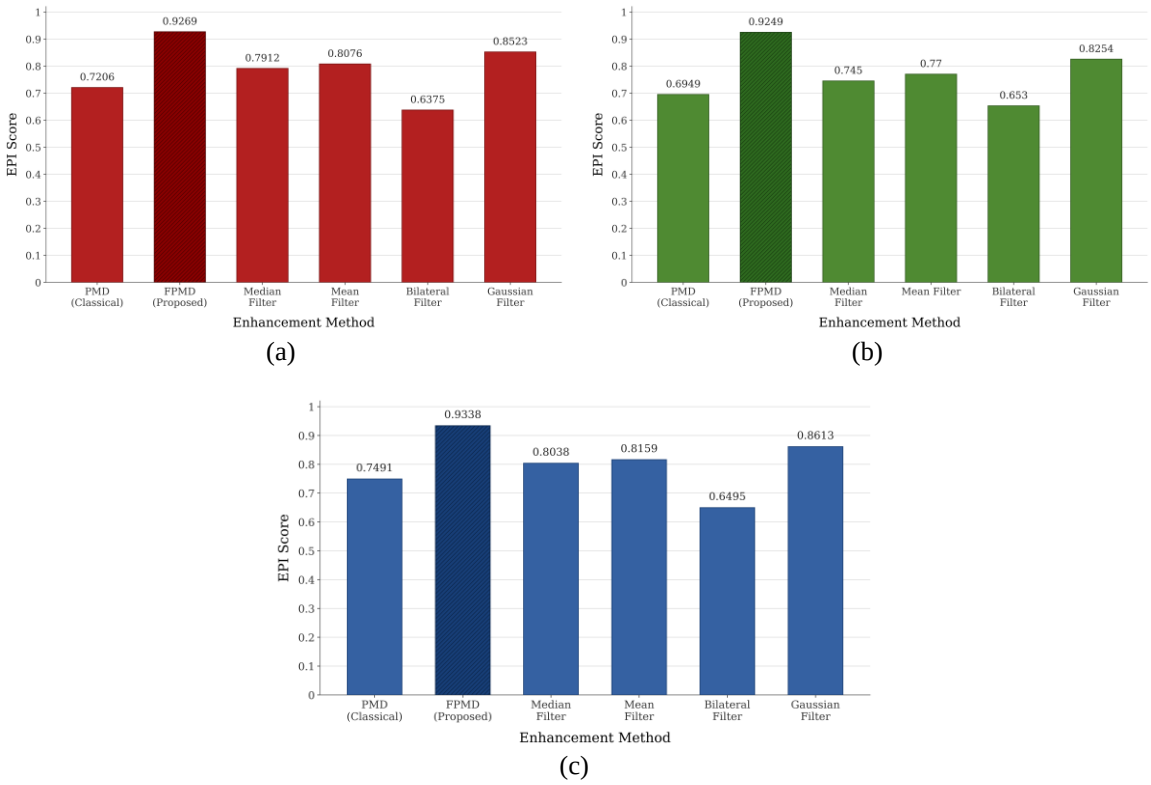

Figure 5. Comparison of the average of EPI score between FPMD filter method, classical PMD filter method and benchmark filtering methods; (a) R channel, (b) G channel, and (c) B channel

Table 1. Average entropy values of Pap smear images after enhancement using classical PMD, proposed FPMD, and benchmark filters for each RGB channel

Enhancement method	Entropy for R channel	Entropy for G channel	Entropy for B channel
Original	6.6098	6.4619	6.3150
PMD (classical)	15.2941	15.0105	14.8250
FPMD (proposed)	15.1451	14.8505	14.6377
Median filter	7.4751	7.3003	7.1505
Mean filter	7.4964	7.3640	7.2179
Bilateral filter	7.4380	7.3411	7.2118
Gaussian filter	7.5012	7.3662	7.2195

Although classical PMD achieves slightly higher entropy than FPMD, this increase is accompanied by a substantial degradation in perceptual quality. Specifically, the BRISQUE score of classical PMD increases to 55.78 (a 56.7% rise compared to the original image), whereas FPMD reduces BRISQUE to 18.88 (a 46.96% improvement), indicating clearer and less distorted visual output. In addition, FPMD provides a 130.23% entropy gain over the original image while improving the EPI by 28.69% relative to classical PMD, demonstrating a better balance between noise suppression and structural preservation. These improvements are attributed to the fractional-order formulation, which enables more adaptive diffusion control and enhanced retention of fine cytological features.

From a computational perspective, however, a significant trade-off is observed. The average processing times are summarized in Table 2. Classical PMD requires 0.5666 s per image, whereas the proposed FPMD requires 97.0409 s, making it substantially slower than both classical PMD and conventional filters (0.44–0.49 s). This increased computational cost is primarily attributed to the iterative implementation of the GL fractional operators. Consequently, although FPMD provides superior enhancement performance, its practical application in real-time or large-scale scenarios may be limited unless computational acceleration strategies, such as GPU parallelization or optimized fractional implementations, are employed.

The visual comparison in Figures 6 and 7 demonstrates the effect of FPMD enhancement across the five cytological classes, with Figure 6 showing the original images and Figure 7 presenting the corresponding enhanced results. In Figures 6(a) and 7(a), dyskeratotic cells are characterized by dense orangeophilic cytoplasm and small hyperchromatic nuclei; after enhancement, the nuclear and cytoplasmic boundaries become more distinct. Figures 6(b) and 7(b) show koilocytotic cells with enlarged irregular nuclei and prominent perinuclear halos, which are more clearly separated from the surrounding cytoplasm after FPMD processing. Figures 6(c) and 7(c) depict metaplastic cells with polygonal shapes, cyanophilic cytoplasm, and relatively uniform central nuclei, while the enhanced images preserve their cellular contours and internal textures. Figures 6(d) and 7(d) present small parabasal cells with scant cytoplasm and a high nucleus-to-cytoplasm ratio, for which FPMD improves nucleus–cytoplasm contrast. Finally, Figures 6(e) and 7(e) show large superficial–intermediate cells with abundant cytoplasm and relatively small nuclei, where cytoplasmic margins and staining variations become more visible after enhancement. Overall, FPMD reduces background noise and nonuniform staining while preserving diagnostically relevant structures, including nuclear contours, perinuclear halos, cytoplasmic boundaries, and cell-specific textures. These improvements can support more reliable visual interpretation and provide higher-quality inputs for subsequent segmentation and classification. However, the present study evaluates only image-enhancement quality; its effect on downstream diagnostic models and its generalizability to whole-slide and larger clinical datasets should be investigated in future work.

Table 2. Average computational time (in seconds) required by each enhancement method during processing of RGB Pap smear images

Enhancement method	Computational time (s)
PMD (classical)	0.5666
FPMD (proposed)	97.0409
Median filter	0.4901
Mean filter	0.4424
Bilateral filter	0.4808
Gaussian filter	0.4475

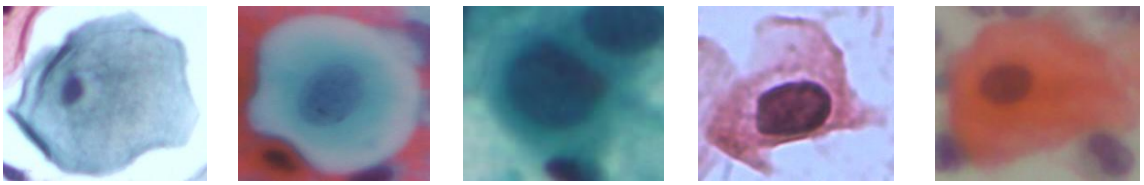

(a) (b) (c) (d) (e)

Figure 6. The example of image before applying the FPMD filter; (a) dyskeratotic class, (b) koilocytotic class, (c) metaplastic class, (d) parabasal class, and (e) superficial-intermediate class

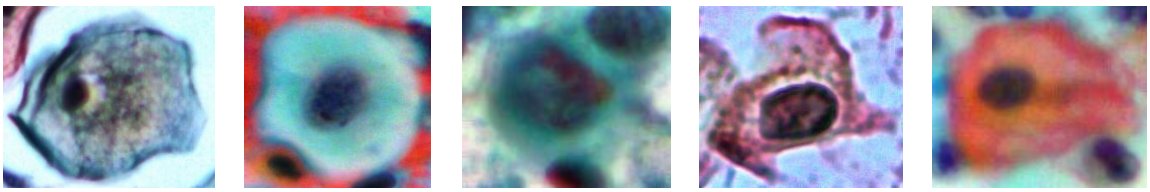

(a) (b) (c) (d) (e)

Figure 7. The example of image after applying the FPMD filter; (a) dyskeratotic class, (b) koilocytotic class, (c) metaplastic class, (d) parabasal class, and (e) superficial-intermediate class

Beyond perceptual improvement, FPMD preprocessing enhances feature extraction, improves classification accuracy, and increases segmentation robustness, thereby strengthening its role in AI-assisted

cervical cancer screening. By producing clearer nuclear boundaries and preserving cytoplasmic textures, FPMD provides higher-quality inputs for downstream tasks such as nucleus–cytoplasm separation, feature learning, and automated cell classification.

From a clinical deployment perspective, FPMD is particularly suitable as an offline or preprocessing module in CAD systems, where diagnostic accuracy is prioritized over real-time performance. Although the method exhibits higher computational complexity than classical PMD and conventional filters, this limitation can be mitigated through batch preprocessing, GPU-based acceleration, or centralized laboratory workflows. In resource-limited screening settings, where image quality is often degraded by noise and uneven staining, the adaptive and structure-preserving properties of FPMD can improve the robustness of AI-assisted decision-making and potentially reduce diagnostic errors.

Nevertheless, the reliance on empirically selected parameters (α, k) and the high computational cost remain open challenges. These limitations motivate future research directions, including automatic parameter optimization and computational acceleration strategies, positioning FPMD as a promising yet evolving preprocessing framework for cytology-based cervical cancer screening.

4. CONCLUSION

The proposed FPMD method demonstrates superior performance in enhancing Pap smear images compared with classical PMD and conventional filters, achieving the lowest BRISQUE score (18.88) and the highest EPI values across the RGB channels. Although the entropy value is slightly lower than that of classical PMD, the resulting enhancement is visually more consistent and preserves diagnostically relevant cellular structures more effectively. Despite these advantages, several limitations should be acknowledged. First, the proposed FPMD method introduces a substantially higher computational cost (97.04 s per image) due to the iterative computation of the GL fractional operators, which limits its applicability in real-time or large-scale screening scenarios. Second, the diffusion parameters were selected empirically rather than through a systematic optimization strategy, which may affect the generalizability of the method across different datasets. Third, the experimental validation was limited to single-cell RGB images and did not include evaluation on WSI data or large multi-center datasets. In addition, the impact of the proposed enhancement method on downstream tasks such as automated cell segmentation or classification was not quantitatively assessed. Future work will therefore focus on several technical directions. Computational acceleration strategies, including GPU-based parallel implementations and optimized fractional discretization schemes, will be explored to reduce the computational burden of the FPMD model. Furthermore, data-driven parameter optimization techniques such as Bayesian optimization or evolutionary algorithms will be investigated to automatically determine optimal diffusion parameters. The proposed framework will also be integrated into end-to-end cervical cytology analysis pipelines that include segmentation and classification modules. Finally, large-scale validation using WSI and cross-institutional clinical datasets will be conducted to evaluate the robustness, scalability, and generalization capability of the proposed method.

ACKNOWLEDGMENTS

The paper's authors are grateful to Brawijaya University's Visiting Lecture Program for their insightful advice, encouragement, and assistance to the advancement of this study.

FUNDING INFORMATION

This research was funded by Brawijaya University.

AUTHOR CONTRIBUTIONS STATEMENT

This journal uses the Contributor Roles Taxonomy (CRediT) to recognize individual author contributions, reduce authorship disputes, and facilitate collaboration.

Name of Author	C	M	So	Va	Fo	I	R	D	O	E	Vi	Su	P	Fu
Syaiful Anam	✓	✓	✓		✓	✓	✓		✓	✓			✓	✓
Normi Abdul Hadi			✓			✓	✓	✓	✓	✓	✓			
Avin Maulana				✓		✓				✓				
Indah Yanti						✓			✓	✓			✓	
Suhaila Abd Halime				✓	✓					✓				

C : **C**onceptualization
M : **M**ethodology
So : **So**ftware
Va : **Va**lidation
Fo : **Fo**rmal analysis
I : **I**nvestigation
R : **R**esources
D : **D**ata Curation
O : Writing - **O**riginal Draft
E : Writing - Review & **E**diting
Vi : **Vi**sualization
Su : **Su**pervision
P : **P**roject administration
Fu : **Fu**nding acquisition

CONFLICT OF INTEREST STATEMENT

We affirm that we don't have any competing interests.

DATA AVAILABILITY

The Pap Smear Single Cell Image Dataset used in this study is publicly accessible on Kaggle at https://www.kaggle.com/datasets/mohaliy2016/papsinglecell.

REFERENCES

[1] M. P. Aulia and M. D. Hartanti, "The effect of cervical cancer counseling on cervical cancer prevention behavior in women of childbearing age: A literature study," *Jurnal Kedokteran Diponegoro (Diponegoro Medical Journal)*, vol. 12, no. 5, pp. 283–292, Aug. 2023, doi: 10.14710/dmj.v12i5.38759.

[2] J. H. Saputra, L. Sary, and N. Muhani, "Cervical cancer screening utilization among women aged 30-49 years in Lampung, Indonesia," *Malahayati International Journal of Nursing and Health Science*, vol. 6, no. 5, pp. 391–398, Nov. 2023, doi: 10.33024/minh.v6i5.12827.

[3] A. Analysa, D. P. O. Lestari, and I. G. A. Artha, "Overexpression of PDL-1 is a risk factor for lymph node metastasis in cervical cancer," *International journal of health & medical sciences*, vol. 6, no. 2, pp. 69–76, Apr. 2023, doi: 10.21744/ijhms.v6n2.2104.

[4] W. Agustina, D. P. Era, and E. E. Urnia, "Determinant factors of behavior of women of reproductive age on early detection of cervic cancer," *KESANS : International Journal of Health and Science*, vol. 3, no. 1, pp. 69–76, Oct. 2023, doi: 10.54543/kesans.v3i1.240.

[5] M. Santosa, A. K. Anjaya, V. D. J. Juliawati, R. Irawan, and Yuliana, "Cervical cancer campaign: Correlation between HPV vaccine and cervical cancer knowledge with HPV vaccination rate," *Journal of Urban Health Research*, vol. 1, no. 3, pp. 1-11, Jul. 2023, doi: 10.25170/juhr.v1i3.4463.

[6] Y. Jia, K. Zou, and L. Zou, "Research progress of metabolomics in cervical cancer," *European Journal of Medical Research*, vol. 28, no. 1, pp. 1-9, Dec. 2023, doi: 10.1186/s40001-023-01490-z.

[7] N. Youneszade, M. Marjani, and C. P. Pei, "Deep learning in cervical cancer diagnosis: Architecture, opportunities, and open research challenges," *IEEE Access*, vol. 11, pp. 6133–6149, 2023, doi: 10.1109/ACCESS.2023.3235833.

[8] Y. Pan, Z. Shen, Y. He, K. Wei, and Y. Zhang, "Application of three-dimensional coding network in screening and diagnosis of cervical precancerous lesions," *Frontiers in Computing and Intelligent Systems*, vol. 6, no. 3, pp. 61–64, Jan. 2024, doi: 10.54097/mi3VM0yB.

[9] P. S. Mitra, A. C. Nag, D. Roy, B. Modak, T. S. Bag, and T. K. Naskar, "Cervical exfoliative cytology by papanicolaou stain and visual inspection with acetic acid in screening of cervical cancer: A cross-sectional observational study," *Journal of Medical Sciences and Health*, vol. 10, no. 1, pp. 65–72, Apr. 2024, doi: 10.46347/jmsh.v10.i1.23.312.

[10] E. I. Obeagu, "Cervical cancer unveiled: Insights into HPV, risks, and therapeutic frontiers," *Cancer Research and Cellular Therapeutics*, vol. 8, no. 1, pp. 01–04, Feb. 2023, doi: 10.31579/2640-1053/181.

[11] H. Khiari, K. Makni, K. Meddeb, O. Jaidane, and M. Hsairi, "Cost-effectiveness of human papillomavirus (HPV) vaccination in Tunisia: a modelling study," *BMJ Open*, vol. 14, no. 12, pp. 1-7, Dec. 2024, doi: 10.1136/bmjopen-2024-085462.

[12] S. Zergeroğlu, Z. S. Özkan, and A. H. Aydin, "Are the correlation results of HPV positive cases with cervical smear always consistent?," *Journal of Medicine and Palliative Care*, vol. 4, no. 2, pp. 158–162, Mar. 2023, doi: 10.47582/jompac.1258024.

[13] S. Etemad *et al.*, "Prevalence of human papillomavirus (HPV) infection and its association with pap smear findings among women attending a gynecology clinic in Khorasan Razavi-Iran," *Journal of Research in Health Sciences*, vol. 24, no. 4, Sep. 2024, doi: 10.34172/jrhs.2024.164.

[14] S. Haridas and T. Jayamalar, "A versatile detection of cervical cancer with I-WFCM and deep learning based RBM classification," *Journal of Machine and Computing*, pp. 238–250, Jul. 2023, doi: 10.53759/7669/jmc202303022.

[15] L. Allahqoli *et al.*, "Diagnosis of cervical cancer and pre-cancerous lesions by artificial intelligence: A systematic review," *Diagnostics*, vol. 12, no. 11, pp. 1-32, Nov. 2022, doi: 10.3390/diagnostics12112771.

[16] C. Suguna and S. P. Balamurugan, "Multi-class segmentation with deep learning based pap smear image analysis for cervical cancer detection and classification model," *Tuijin Jishu/Journal of Propulsion Technology*, vol. 44, no. 3, pp. 4475–4487, Nov. 2023, doi: 10.52783/tjjpt.v44.i3.2453.

[17] A. Khozaimi, I. Darti, S. Anam, and W. M. Kusumawinahyu, "Advanced cervical cancer classification: Enhancing pap smear images with hybrid PMD filter-CLAHE," *Indonesian Journal of Electrical Engineering and Computer Science*, vol. 39, no. 1, pp. 644–655, Jul. 2025, doi: 10.11591/ijeecs.v39.i1.pp644-655.

[18] F. Efil and Z. Cömert, "Filter-based image enhancement effects on CNN-based decision support system for cervical cancer diagnosis," in *2024 8th International Symposium on Multidisciplinary Studies and Innovative Technologies (ISMSIT)*, Nov. 2024, pp. 1–4, doi: 10.1109/ISMSIT63511.2024.10757218.

[19] Rudiansyah, A. Desiani, D. P. Rini, L. I. Kesuma, F. Salamah, and S. C. Putri, "Median filter and U-net architecture for robust segmentation nucleus and cytoplasm on pap smear," in *2024 International Conference on Informatics, Multimedia, Cyber and Information System (ICIMCIS)*, Nov. 2024, pp. 779–784, doi: 10.1109/ICIMCIS63449.2024.10956522.

[20] T. Sood, P. Khandnor, and R. Bhatia, "Enhancing pap smear image classification: integrating transfer learning and attention mechanisms for improved detection of cervical abnormalities," *Biomedical Physics & Engineering Express*, vol. 10, no. 6, Nov. 2024, doi: 10.1088/2057-1976/ad7bc0.

[21] C. Macancela, M. E. Morocho-Cayamcela, and O. Chang, "Deep reinforcement learning for efficient digital pap smear analysis," *Computation*, vol. 11, no. 12, pp. 1-20, Dec. 2023, doi: 10.3390/computation11120252.

[22] A. Charkaoui and A. Ben-loghfyry, "Anisotropic equation based on fractional diffusion tensor for image noise removal," *Mathematical Methods in the Applied Sciences*, vol. 47, no. 12, pp. 9600–9620, Aug. 2024, doi: 10.1002/mma.10085.
[23] J. Wei, X. Liao, and H. Zhou, "Directional Laplacian-based fractional anisotropic diffusion for noise removal in image processing," *Nonlinear Dynamics*, vol. 113, pp. 13913–13929, 2025, doi: 10.1007/s11071-025-10870-5.
[24] T. Huang, X. Wang, D. Xie, C. Wang, and X. Liu, "Depth image enhancement algorithm based on fractional differentiation," *Fractal and Fractional*, vol. 7, no. 5, pp. 1-21, May 2023, doi: 10.3390/fractalfract7050394.
[25] H. Zhang *et al.*, "Learnable PM diffusion coefficients and reformative coordinate attention network for low dose CT denoising," *Physics in Medicine & Biology*, vol. 68, no. 24, Dec. 2023, doi: 10.1088/1361-6560/aced33.
[26] A. Mustafa, O. Ragb, M. Salah, R. S. Salama, and M. Mohamed, "Distinctive shape functions of fractional differential quadrature for solving two-dimensional space fractional diffusion problems," *Fractal and Fractional*, vol. 7, no. 9, pp. 1-22, Sep. 2023, doi: 10.3390/fractalfract7090668.
[27] R. Banerjee, R. K. Chatterjee, and A. Kar, "An image inpainting model for grayscale images based on TV-H-1 coupled with perona-malik equation," *Journal of Applied Mathematics and Computation*, vol. 7, no. 1, pp. 152–161, May 2023, doi: 10.26855/jamc.2023.03.017.
[28] S. M. Pizer, R. E. Johnston, J. P. Ericksen, B. C. Yankaskas, and K. E. Muller, "Contrast-limited adaptive histogram equalization: speed and effectiveness," in *[1990] Proceedings of the First Conference on Visualization in Biomedical Computing*, 1990, pp. 337–345, doi: 10.1109/VBC.1990.109340.
[29] X. Li, Q. Yu, X. Pan, and Z. Yu, "Research on the contrast enhancement algorithm for X-ray images of BiFeO3 material experiment," *Applied Sciences*, vol. 14, no. 9, pp. 1-17, Apr. 2024, doi: 10.3390/app14093546.
[30] A. Mittal, A. K. Moorthy, and A. C. Bovik, "No-reference image quality assessment in the spatial domain," *IEEE Transactions on Image Processing*, vol. 21, no. 12, pp. 4695–4708, Dec. 2012, doi: 10.1109/TIP.2012.2214050.
[31] P. Perona and J. Malik, "Scale-space and edge detection using anisotropic diffusion," *IEEE Transactions on Pattern Analysis and Machine Intelligence*, vol. 12, no. 7, pp. 629–639, Jul. 1990, doi: 10.1109/34.56205.
[32] Y. Dimitrov, S. Georgiev, and V. Todorov, "Approximation of caputo fractional derivative and numerical solutions of fractional differential equations," *Fractal and Fractional*, vol. 7, no. 10, pp. 1-26, Oct. 2023, doi: 10.3390/fractalfract7100750.
[33] A. Luque-Chang, E. Cuevas, A. Chavarin, and M. Perez, "Agent-based image contrast enhancement algorithm," *IEEE Access*, vol. 11, pp. 6060–6077, 2023, doi: 10.1109/ACCESS.2023.3237086.
[34] N. Nazir, A. Sarwar, and B. S. Saini, "PAP-Net: A systematic framework for denoising pap smear images," *SN Computer Science*, vol. 6, no. 5, May 2025, doi: 10.1007/s42979-025-03977-4.

BIOGRAPHIES OF AUTHORS

Syaiful Anam received a Doctor of Natural Science and Mathematics degree from Yamaguchi University, Japan in 2015. He also received his Master Degree in multimedia intelligence networks from Sepuluh Nopember Institute of Technology, Indonesia in 2006. He is currently an associate professor at Department of Mathematics, Brawijaya University, Malang, Indonesia. His research includes data science, computational intelligence, machine learning, digital image processing, and computer vision. He can be contacted at email: syaiful@ub.ac.id.

Normi Abdul Hadi received her first and Master degrees in Mathematics from Universiti Sains Malaysia (USM), 2005 - 2006. Her Ph.D. is in Computational Mathematics in 2015 from Universiti Teknologi MARA (UiTM), Malaysia. Her research interest is in computer aided geometric design (CAGD). Currently, she focuses on CAGD in 3D point clouds and parallel computing. She can be contacted at email: normi683@uitm.edu.my.

Avin Maulana received his master degree in Informatics Engineering from Sepuluh Nopember Institute of Technology in 2020. He also received his Bachelor Degree in Mathematics from Brawijaya University, Indonesia in 2018. He is a Lecturer at Mathematics Department, Brawijaya University, Malang, Indonesia. His research interests include machine learning and deep learning. He can be contacted at email: avin_maulana@ub.ac.id.

Indah Yanti received her master degree in Mathematics from Brawijaya University in 2012. She also received his Bachelor Degree in Mathematics from Brawijaya University, Indonesia in 2003. She is a Lecturer at Mathematics Department, Brawijaya University, Malang, Indonesia. Her research interests include computer vision, image processing, and data science. She can be contacted at email: indah_yanti@ub.ac.id.

Suhaila Abd Halime received her Ph.D. degree in Mathematics from Ph.D. from Universiti Teknologi MARA (UiTM) in 2017. She is an associate professor at Faculty of Computer and Mathematical Sciences, Universiti Teknologi MARA (UiTM), Malaysia. Her research interests include image processing and numerical method. She can be contacted at email: suhaila889@uitm.edu.my.